Journal of
Sensor and Actuator Networks

MDPI

Article

Uncoupled Wi-Fi Body CoM Acceleration for the Analysis of Lightweight Glass Slabs under Random Walks

Chiara Bedon * and Salvatore Noè

Department of Engineering and Architecture, University of Trieste, 34127 Trieste, Italy; noe@units.it
* Correspondence: chiara.bedon@dia.units.it

Abstract: The vibration serviceability assessment of slender and/or lightweight pedestrian systems with high sensitivity to walk-induced effects is rather challenging. In the same way, laminated glass (LG) is used in buildings for structural applications but still represents a not well known and vulnerable material. For pedestrian LG systems, the characterization of dynamic and mechanical parameters may require specific procedures which do not adapt from other constructional typologies. Among others, the mass of pedestrians is generally high compared with LG structural components. Size and restraints in LG may also lead to more pronounced vibration effects. For existing LG systems, moreover, knowledge of residual capacity may be rather difficult. In this paper, an original uncoupled experimental investigation is proposed to numerically address the accuracy and potential of low-cost laboratory body measures for vibration analysis of LG slabs to support (or even replace) field tests or more complex calculation approaches. A total of 40 experimental records are taken into account, in the form of body center of mass (CoM) acceleration time histories for an adult volunteer walking on a rigid concrete slab and equipped with a single high-precision, Wi-Fi triaxial sensor based on micro electromechanical systems (MEMS) technology. Body CoM records are elaborated and used as input for finite element (FE) nonlinear dynamic analysis in the time domain (WL1) of two LG slab configurations (GS1 and GS2) with identical geometry but different boundaries. A third reinforced concrete slab of literature (CS3) is also investigated for further assessment. Numerical parametric results from a total of 120 WL1-based nonlinear dynamic analyses are compared with FE numerical results based on a conventional deterministic approach (WL2) to describe walk-induced effects, as well as towards past field experiments (GS2). The accuracy and potential of the proposed procedure are discussed.

Keywords: slabs; vibrations; laminated glass (LG); body center of mass (CoM); micro electromechanical systems (MEMS) sensor; experiments; numerical modeling

Citation: Bedon, C.; Noè, S. Uncoupled Wi-Fi Body CoM Acceleration for the Analysis of Lightweight Glass Slabs under Random Walks. *J. Sens. Actuator Netw.* **2022**, *11*, 10. https://doi.org/10.3390/jsan11010010

Academic Editor: Thomas Newe

Received: 19 December 2021
Accepted: 26 January 2022
Published: 27 January 2022

1. Introduction

Structural glass is often used in flooring systems to cover wide transparent surfaces. Typical applications consist in triple-laminated glass (LG) sections linearly supported along the four edges by frames acting as rigid bracers. In doing so, LG modular units are designed under quasi-static equivalent actions to satisfy ultimate and serviceability performance indicators based on robustness and redundancy principles [1–3]. Besides, there is often the need to increase the grid size, and/or minimize the presence of bracing frames, or even use point-fixing restraints in place of continuous restraints (Figure 1a). These conditions could result in additional flexibility for LG modules, and thus potential sensitivity increase, towards human-induced vertical loads. Compared with traditional slabs in concrete, for example, there is a strong modification of mechanical and dynamic parameters for LG systems, and thus possible critical response to walks. Additional uncertainty for LG under pedestrian effects is represented by the use of bonding interlayers, which are characterized by a remarkable viscoelastic response to time loading, temperature, ambient conditions, and thus by progressive modification in mechanical features of the composite-resisting

cross-section [4,5]. Basic equivalent mechanical properties can be used for interlayers, especially for LG systems suffering from severe degradation phenomena [6].

In this regard, the combination of these multiple aspects requires special attention for the analysis of possible vibration issues in LG pedestrian modules under random walks. Actually, there is limited research in support of appropriate and holistic analysis and verification of vibration performances for LG pedestrian structures. The few available experimental and numerical investigations confirm their high sensitivity to human-induced effects, especially for in-service structures affected by long-term phenomena [7–10].

The description and measure of body movements is well known to represent a rather complex topic. Many literature research studies have been dedicated to the analysis of reaction forces due to pedestrians, in support of vibration serviceability analysis of various slab systems [11–13]. A number of research investigations have also been proposed to assess the potential and reliability of various types of sensors for the measure of walking parameters in pedestrians [14–16]. The efficient use of multiple body sensors to capture motion records for the estimation of the vertical ground reaction force of pedestrians has been assessed in [17,18] for structural vibration purposes, see Figure 1b. Bocian et al. [19] proved experimentally that a single point inertial measurement can accurately capture the pedestrian vertical-induced force. Based on laboratory-measured pedestrian histories and field walking tests on a real bridge, the simulated response of a bridge under uncoupled body records was efficiently captured.

(**a**) (**b**) (**c**)

Figure 1. Example of (**a**) point-fixed glass floor and (**b**,**c**) use of sensors to capture body motion and walking parameters in laboratory conditions (image (**b**) reproduced from [17] with permission from Elsevier®, license number 5222960756537, January 2022; image (**c**) reproduced from [20] under CC-BY license agreement).

Many aspects are known to typically affect walking features—and thus induced vertical forces—for a given pedestrian, including age, medical issues, etc. [20], see Figure 1c. In addition, input walking features can mutually interact with basic structural parameters of supporting slabs [21,22], and severe human–structure interaction is expected for some potential critical design solutions, such as in LG applications.

To overcome this open challenge, the present study explores the potential and accuracy of uncoupled, low-cost Wi-Fi measures of walking occupants, so as to capture relevant motion features in support of refined, computationally efficient vibration analyses of LG slabs.

2. Research Methods

Structurally speaking, the nonlinear numerical analysis of human-induced dynamic effects on pedestrian components attracted several studies in recent decades, focused on the definition of efficient and reliable models to describe pedestrians [23]. Among others, deterministic models as in [11–13] are characterized by simplicity for application to general slabs under vibrations, once the pedestrian mass M and the walking frequency f_s are known. On the other side, intrinsic uncertainties may derive from motion complexity/variability and structure–pedestrian interaction (walking speed v_s, stride length L_s, damping ξ, etc.). Psychological human comfort (and thus corresponding walking features) may also be further affected by LG transparency [24,25].

The present study investigates the effect of uncoupled random walks on the vibration performance of LG slab modules which can be highly sensitive to pedestrian activities. The procedure is based on a single high-precision micro electromechanical systems (MEMS) sensor in the body center of mass (CoM) of pedestrians, based on laboratory measurements, and their validation to field measurements. Relatively wide surfaces are typically covered with rather small thicknesses of glass. As such, the structural mass (M_{TOT}) is generally low compared with occupants (M). Moreover, depending on mechanical restraints, a given LG slab may be characterized by high flexibility, and thus critical/low fundamental frequency f_1 to vertical excitations, with respect to conventional ranges of walks ($f_s \approx 1.5$–2 Hz). Differing from previous studies, an original uncoupled experimental and finite element (FE) numerical investigation is thus proposed in this paper (Figure 2).

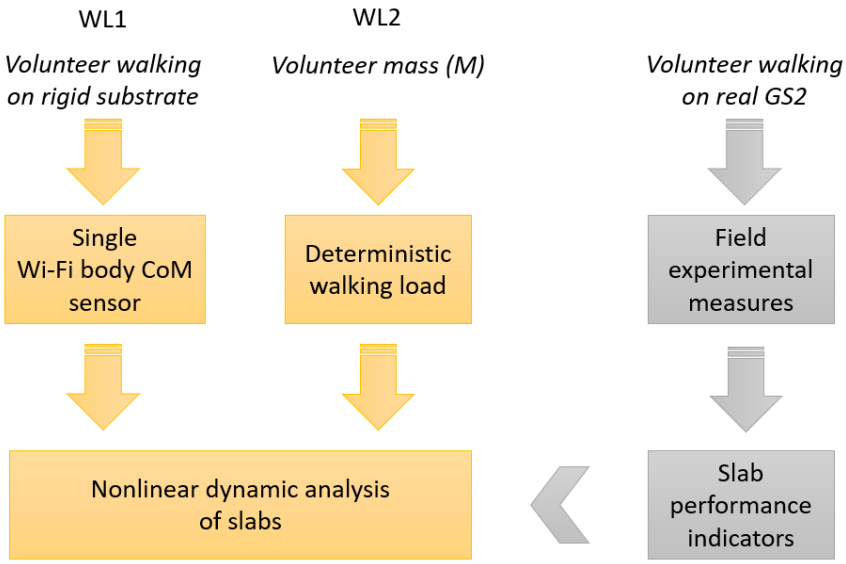

Figure 2. Working procedure for the uncoupled vibration analysis and validation of results.

The attention is in fact primarily focused on the characterization of walk-induced effects, as well as on the analysis of body CoM motion variability on the vibration analysis of slabs which may suffer for higher sensitivity. The presented procedure is based on input acceleration time histories collected in a laboratory framework and used for the FE nonlinear analysis of LG slabs in time domain (WL1). The overall investigation is based on a single volunteer asked to walk on a rigid substrate (laboratory foundation system, Section 3), equipped with a Wi-Fi sensor to capture relevant motions of body CoM.

Two different LG slab configurations are studied (GS1 and GS2). For validation, a third reinforced concrete slab (CS3) is also analyzed. For comparative purposes, the CoM-based numerical vibration analysis of GS1, GS2, and CS3 slabs is addressed towards a consolidated procedure [11,12] for the description of human-induced loads (WL2).

Further assessment of WL1 accuracy and outcomes is proposed, for GS2, on the basis of past field experiments presented in [9] for the real GS2 slab under walks of the same

volunteer (Figure 2). The comparison of present parametric results shows that the uncoupled input from a single body CoM sensor, as also in line with [16], can provide useful feedback in support of efficient vibration analysis of various structural slabs. For LG pedestrian systems characterized by limited structural mass, moreover, the use of deterministic pedestrian loads may result in unsafe predictions of maximum walk-induced effects.

3. Description of Walk-Induced Effects

3.1. Experimental Setup and Record Acquisitions (WL1)

The experimental study presented herein involved a single volunteer (38-year-old female, with M = 80 kg as the weight, H = 1.85 m as the total height, and h = 1.10 m as the the CoM height) asked to walk straight on a rigid concrete floor and to cover a total distance of L = 10–15 m. In doing so, a high-precision, Wi-Fi triaxial sensor was used to track acceleration and inclination time histories (BeanDevice® Wilow® type [26] based on micro electromechanical systems (MEMS) technology for structural health monitoring [27]). The sampling rate was set at 200 Hz and a lumbar belt was used to keep the sensor in position during body motion (Figure 3).

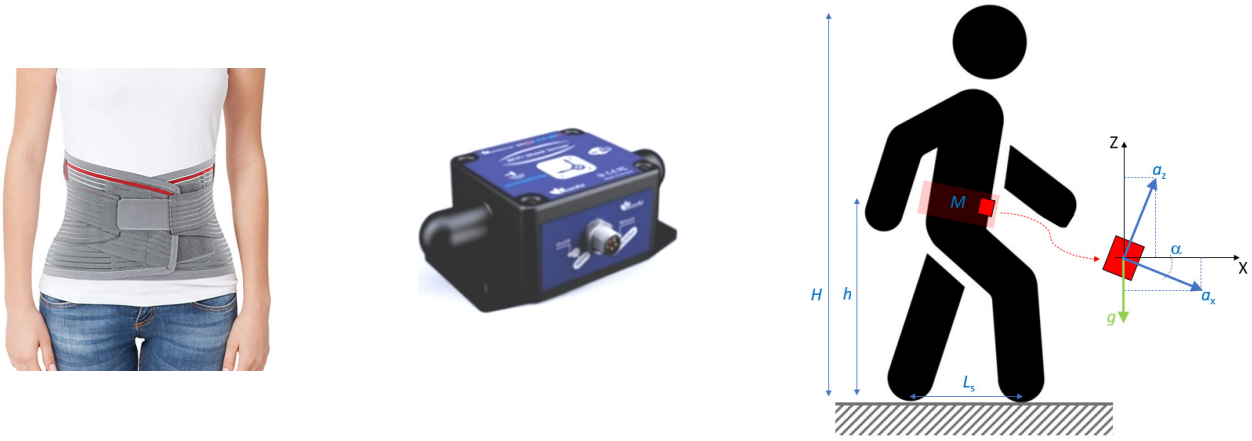

(**a**) (**b**) (**c**)

Figure 3. Experimental methods: (**a**) lumbar belt to keep in position the (**b**) used Wi-Fi sensor and (**c**) reference system for the measure of CoM motion records.

In total, 40 walks were measured under various movement frequencies f_s. All the walks were recorded in laboratory conditions, moving on a rigid concrete foundation slab. The volunteer was asked to walk unrestrainedly and keep rather constant speed, naturally slow or fast, during each test repetition. For each walking configuration, a minimum of 10 steps was taken into account as a reference. This resulted in a total of more than 400 recorded gaits for structural vibration analysis.

Assuming the sensor oriented as in Figure 3c, the vertical acceleration component $a_Z(t)$ during walks was first calculated by taking into account the sensor inclination due to body movements, thus [16]:

$$a_Z(t) = a_z(t)cos\alpha(t) - a_x(t)sin\alpha(t) \quad (1)$$

A typical acceleration record is proposed in Figure 4, while experimental outcomes are further elaborated in Section 3.3.

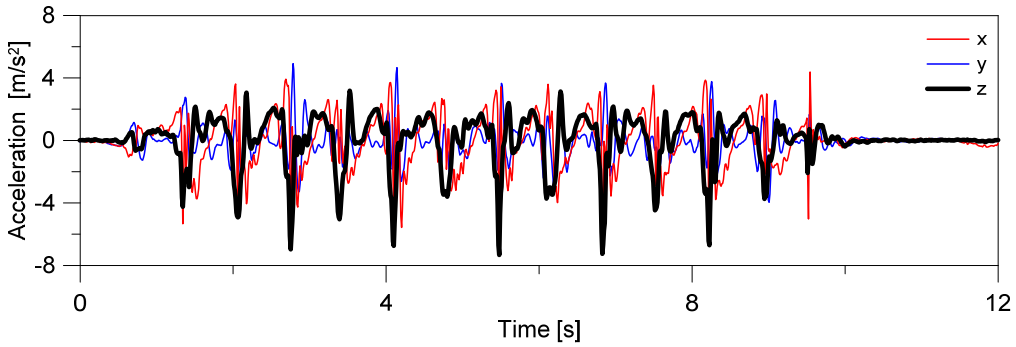

Figure 4. Example of experimental records for CoM accelerations in time.

3.2. Deterministic Numerical Model (WL2)

As a reference for numerical modeling, the consolidated analytical proposal by [11,12] was taken into account for the present investigation. The single footfall is assumed to transfer a force time history equal to (in Newton):

$$F(t) = 746 \sum_{i=1}^{8} K_i t^i = 746\left(K_1 t + K_2 t^2 + K_3 t^3 + K_4 t^4 + K_5 t^5 + K_6 t^6 + K_7 t^7 + K_8 t^8\right) \quad (2)$$

with K_i the coefficients in Table 1 and t the time (in seconds) within a single footfall, where:

$$t_s = -0.515 f_s^3 + 3.2242 f_s^2 - 6.9773 f_s + 5.8531 \quad (3)$$

denotes the duration of a single footfall (in seconds) of walking frequency f_s (in Hertz), see Figure 5a. The corresponding walking speed is given by:

$$v_s = 1.67 f_s^2 - 4.83 f_s + 4.5 \quad (4)$$

Key parameters for a realistic walking path as in Figure 5b are the time overlap of subsequent footfalls (t_o), the length of steps (L_s):

$$t_o = t_s - \frac{1}{f_s} \quad (5)$$

$$L_s = \frac{v_s}{f_s} \quad (6)$$

and the lateral distance of footfalls (D_s = 0.2 m). Besides, depending on structural features, first calculations can also be carried out with footfalls fixed in the most vulnerable region.

Table 1. Definition of input coefficients K_i for Equation (2), based on walking frequency f_s.

Coefficient	f_s (Hz)		
	≤1.75	**1.75 ÷ 2**	**≥2**
K_1	$-8\,f_s + 38$	$24\,f_s - 18$	$75\,f_s - 120$
K_2	$376\,f_s - 844$	$-404\,f_s + 521$	$-1720\,f_s + 3153$
K_3	$-2804\,f_s + 6025$	$4224\,f_s - 6274$	$17{,}055\,f_s - 31{,}936$
K_4	$6308\,f_s - 16{,}573$	$-29{,}144\,f_s + 45{,}468$	$-94{,}265\,f_s + 175{,}710$
K_5	$1732\,f_s - 13{,}619$	$109{,}976\,f_s - 175{,}808$	$298{,}940\,f_s - 553{,}736$
K_6	$-24{,}638\,f_s + 16{,}045$	$-217{,}424\,f_s + 353{,}403$	$-529{,}390\,f_s + 977{,}335$
K_7	$31{,}836\,f_s - 33{,}614$	$212{,}776\,f_s - 350{,}259$	$481{,}665\,f_s - 888{,}073$
K_8	$-12{,}948\,f_s + 15{,}532$	$-81{,}572\,f_s + 135{,}624$	$-174{,}265\,f_s + 321{,}008$

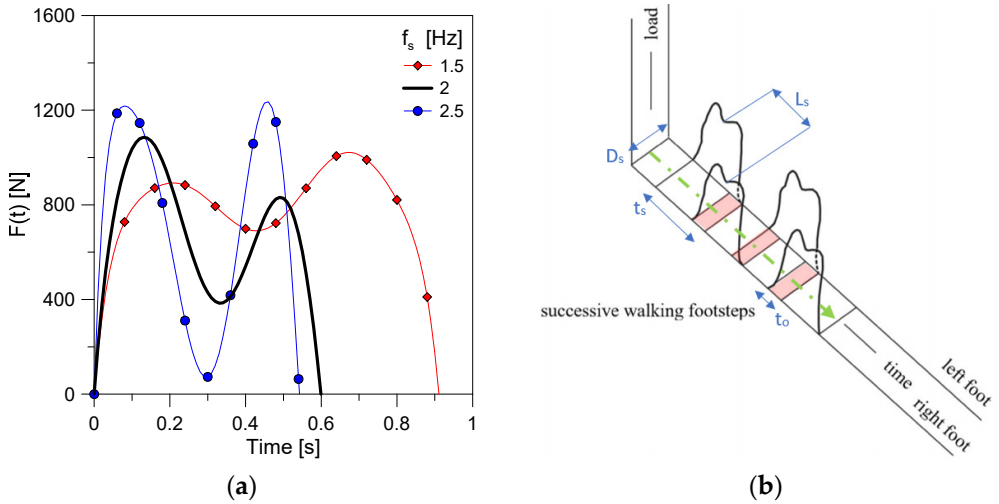

(**a**) (**b**)

Figure 5. Description of footfall loads based on Equation (2): (**a**) typical variation of walking frequency and (**b**) spatial/timing effects.

3.3. Characteristics of Experimental Laboratory Walks

The experimental outcomes from Section 3.1 were further elaborated in Matlab to obtain Frequency Response Function (FRF) and Power Spectral Density (PSD) of signals, walking frequency f_s, and other relevant motion parameters. Figure 6 shows an example of FRF magnitude for one of the collected records, while a summary of parametric experimental data is shown in Figure 7. Finally, Tables 2 and 3 summarize some further walking characteristics, with the R correlation coefficient from the linear regression models as in Figure 7. The gait length L_s was calculated on the base of covered distance L divided by the number of steps n_s for each repetition. The walking speed vs. was measured as gait length L_s multiplied by walking frequency f_s.

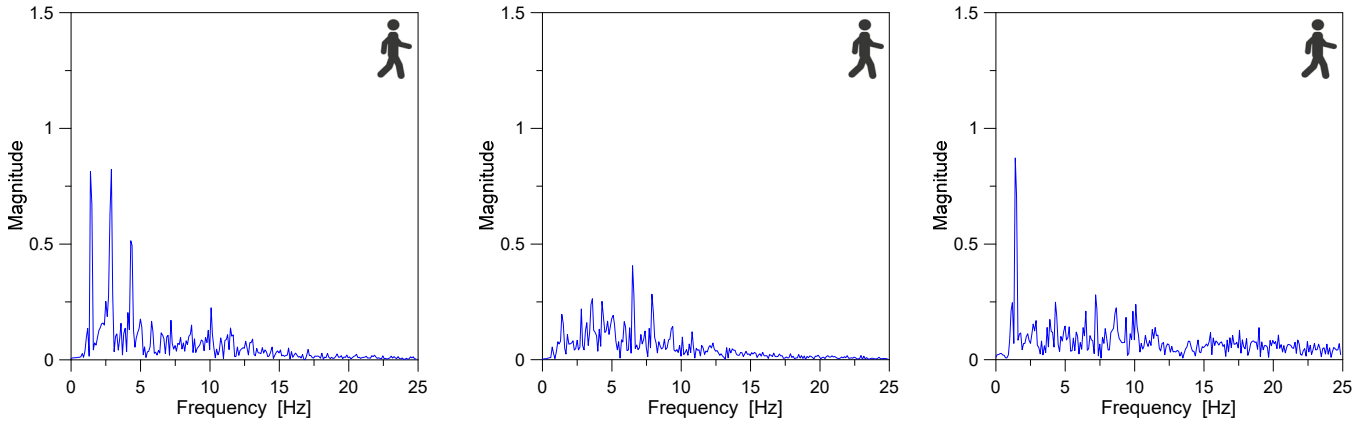

(**a**) (**b**) (**c**)

Figure 6. Example of experimental body CoM acceleration records in terms of FRF magnitude, with evidence of (**a**) vertical; (**b**) transversal; and (**c**) longitudinal components.

Table 2. Statistical analysis of body CoM records, with standard deviation in brackets and R correlation coefficient.

Samples	Frequency		Length		Velocity	
	f_s (Hz)	Range (Hz)	L_s (m)	R	v_s (m/s)	R
40	1.517 (±0.153)	1.248–1.769	0.702 (±0.124)	0.66	1.078 (±0.270)	0.84

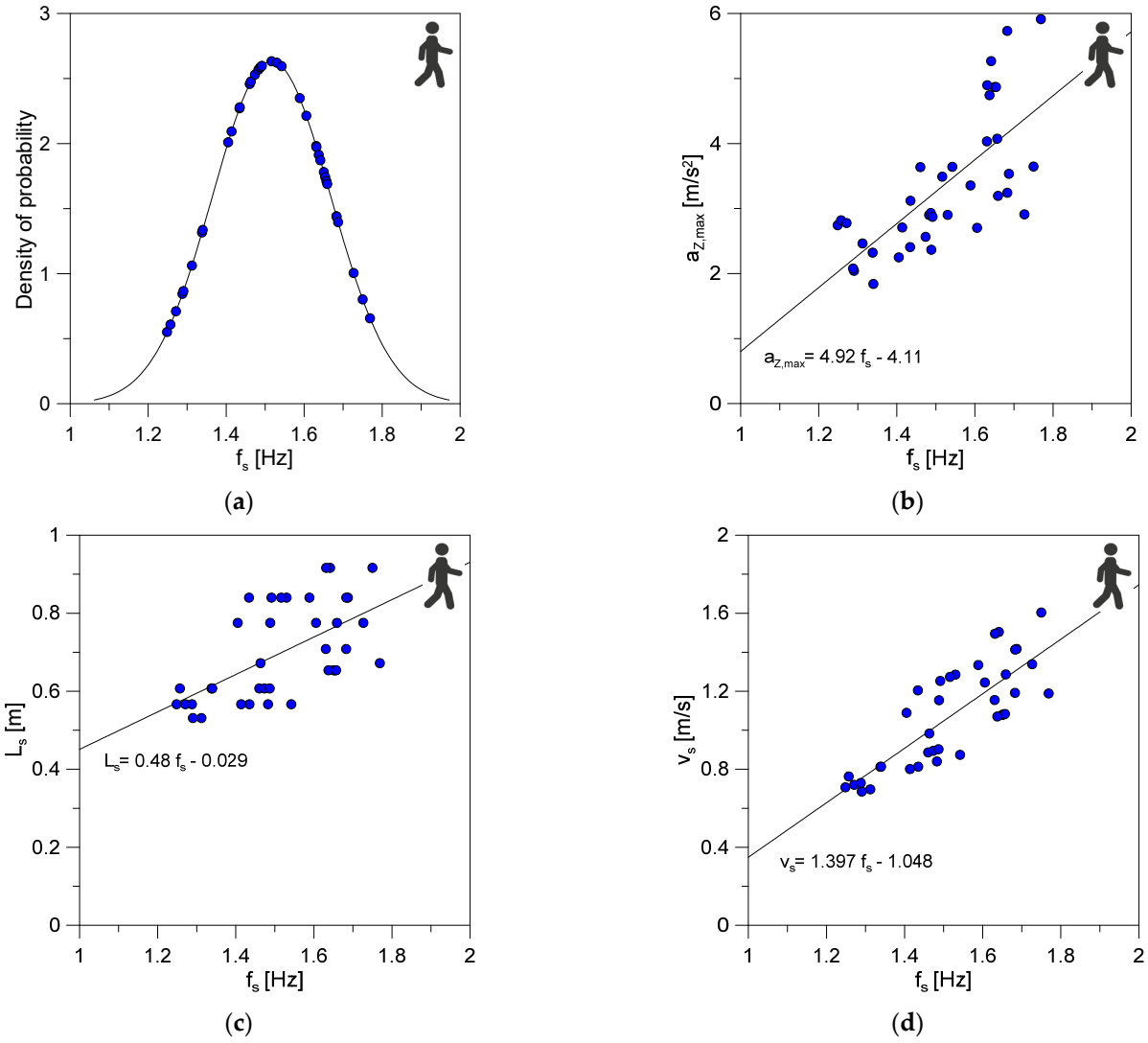

Figure 7. Summary of experimental records as a function of calculated walking frequency f_s: (**a**) Gaussian distribution of samples; (**b**) peak of vertical acceleration component (based on Equation (1)); (**c**) stride length; and (**d**) walking speed.

Table 3. Statistical analysis of body CoM records (vertical acceleration component), with standard deviation in brackets and *R* correlation coefficient.

Samples	Peak			Average		Peak-to-Peak	
	(m/s^2)	Range (m/s^2)	*R*	(m/s^2)	*R*	(m/s^2)	*R*
40	3.348 (±1.057)	1.840–5.913	0.71	0.0032 (±0.003)	0.34	6.219 (±1.736)	0.75

The average walking frequency was measured at 1.51 Hz (±0.16 Hz), see Figure 7a. Further walking characteristics, such as vertical acceleration peak $a_{Z,max}$ (absolute value based on Equation (1)), gait length L_s, and walking speed v_s, are shown in Figure 7b–d as a function of measured f_s values.

According to Figure 7 and Tables 2 and 3, it is possible to see the high variability of walk-induced effects for the same volunteer. The corresponding effects on the structural side are thus assessed in Section 5, and compared with deterministic pedestrian load models.

Figure 8, in this regard, shows the correlation of stride length L_s and walking speed v_s, as obtained from experimental records or deterministic model. The comparative plots

propose the experimentally derived walking parameters on the y-axis, for all the collected records. For each one of them, based on knowledge of f_s, the corresponding parameters given by Equations (4) and (6) are proposed on the x-axis. As expected, it is possible to see the high variability and sensitivity of walking features for the single involved subject, and thus the weak correlation of examined indicators based on the walking frequency only.

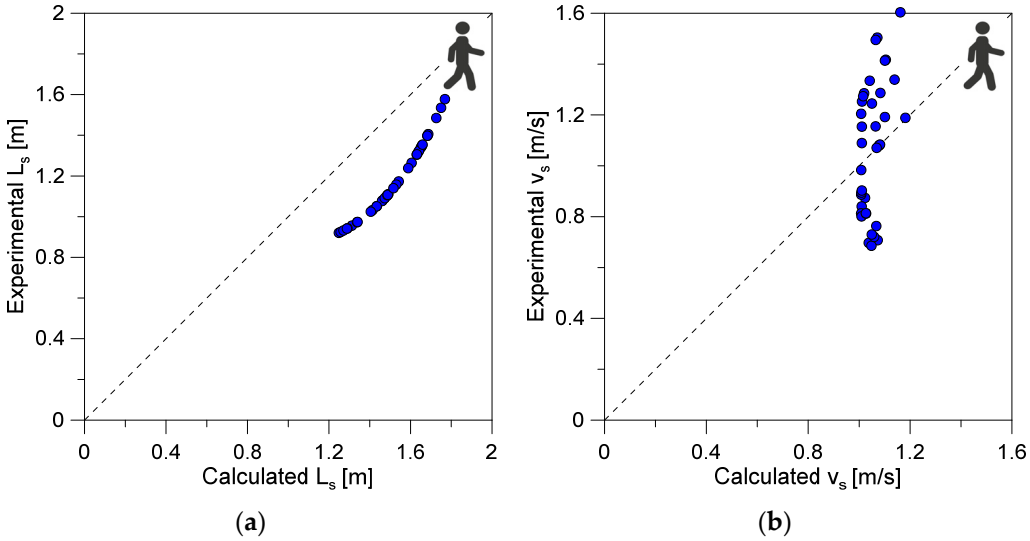

Figure 8. Comparison of experimentally derived walking parameters compared with deterministic models, in terms of (**a**) stride length (based on Equation (6)) or (**b**) walking speed (from Equation (4)).

4. Finite Element Numerical Analysis

A parametric numerical analysis was carried out in ABAQUS software [28], to investigate the effects of human-induced accelerations on the vibration response of a LG slab system. To this aim, two different configurations were taken into account (GS1 and GS2, in the following) and two loading strategies (WL1 and WL2). Further assessment of body CoM input was carried out towards the concrete slab (CS3) investigated in [29] by Cai et al. under random walks.

4.1. Slab Features and Modelling

For the analysis of LG slabs, the panel in Figure 9a was taken into account to inspire the present investigation, due to the availability of earlier numerical validation and past field test measurements on the structural side [8–10], based on operational modal analysis techniques. An intrinsic advantage of the existing case-study system was also represented by past demonstration of long-term effects on bonding layers for glass panels, and thus on the efficient mechanical characterization of PVB® layers with an equivalent secant stiffness modulus which was dynamically identified in [8–10].

More precisely, two different slab systems were inspired by Figure 9 and examined under random walks, by taking into account a total dimension $A = 1.35 \times B = 2.65$ m (with 3.58 m^2 of pedestrian surface) and a nominal cross section consisting of fully tempered (FT) glass layers (3 layers × 12 mm) with interposed PVB foils (0.76 mm). The characteristic of the original system in Figure 9a is that an additional protective layer made of annealed (AN) glass (6 mm in thickness) is positioned on the LG top surface (details of Figure 9b). The mechanical interaction between LG and the top AN layer is offered by contact only.

For the current parametric analysis, the following GS1 and GS2 slab systems were thus considered (Figure 10):

- GS1 = linear supports along the B edges of LG module, with A edges unrestrained.
- GS2 = linear supports along the short A edges of LG module. In this case, two pairs of pre-stressed tendons (AISI 316 steel, 10 mm diameter), installed at mid-span with

mechanical unilateral point fixings, were also taken into account to avoid large bending deformations due to vertical loads from pedestrians [9].

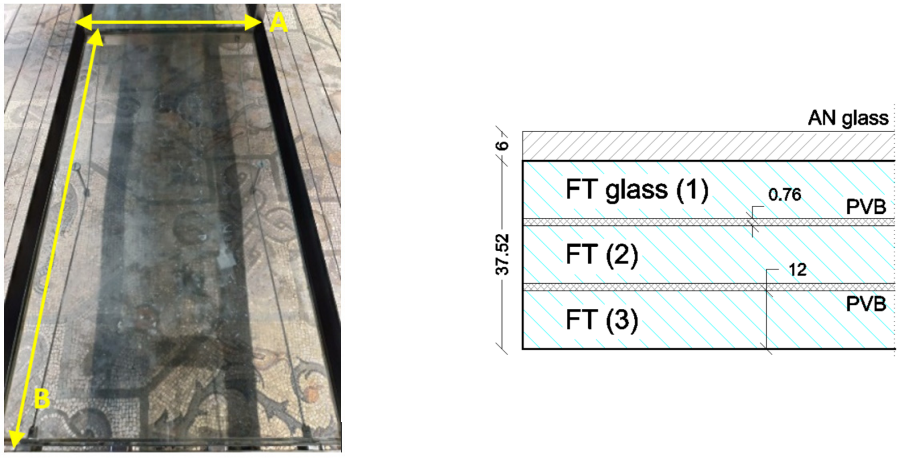

(**a**) (**b**)

Figure 9. Reference in-service laminated glass slab inspiring the present study [9]: (**a**) top view and (**b**) nominal cross section (values in mm).

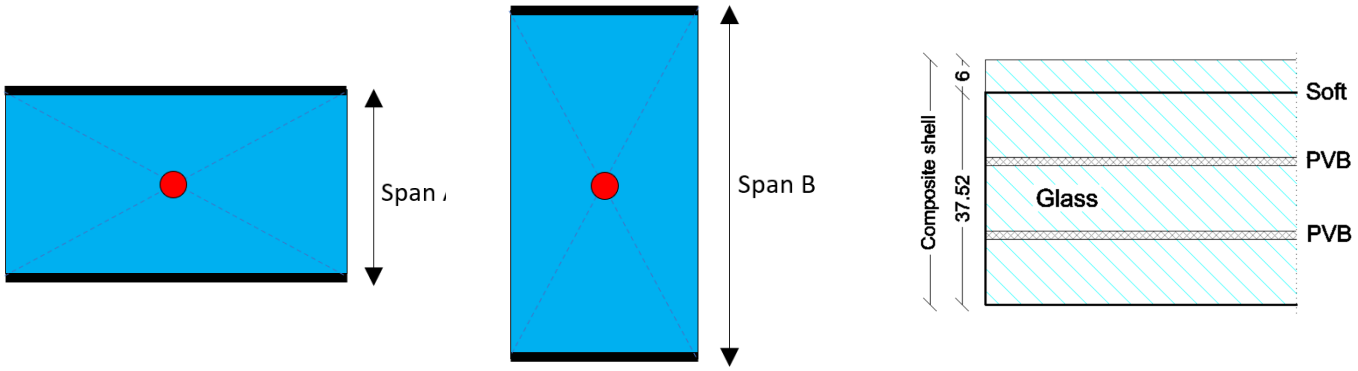

(**a**) (**b**) (**c**)

Figure 10. Examined laminated glass slabs: (**a**) GS1, (**b**) GS2, and (**c**) composite shell description (values in mm).

For the nonlinear dynamic analysis, both GS1 and GS2 were numerically described by a set of "composite" shell elements (S4R type) reproducing the cross section of glass (3 layers × 12 mm glass layers and 2 × 0.76 mm PVB foils) and the sustained AN cover (Figure 10b). The typical FE assembly was discretized with a regular mesh pattern having an average edge size of ≈40 mm. For GS2, beam elements (B31 type) were also used for the steel tendons, to account for their nominal circular section (10 mm the diameter). Linear elastic constitutive laws were used based on [9], to describe glass, PVB, and steel components (Table 4).

Table 4. Input material properties for GS1 and GS2 models.

Material Property	Unit	Glass	Interlayer	Steel (for GS2 Only)
Modulus of elasticity	MPa	70000	4	160000
Poisson's ratio	-	0.23	0.49	0.3
Density	kg/m^3	2500	1100	7850

The examined GS1 and GS2 slab systems with geometry as in Figure 10 were characterized by a total mass M_{TOT} = 320 kg, that is R_M = 4 times the volunteer weight.

The preliminary stage of analysis included a linear elastic estimate of vibration modes for the examined slabs (Figure 11). Due to modification in boundary conditions as in Figure 10a,b, the fundamental vibration frequency of the occupied slabs (with M = 80 kg lumped in the center) resulted in $f_{1,GS1}$ = 51.2 Hz and $f_{1,GS2}$ = 14.3 Hz, respectively, for the first vibration mode (Figure 11a,b), and $f_{2,GS1}$ = 53.2 Hz and $f_{2,GS2}$= 33.2 Hz for the second mode (Figure 11c,d).

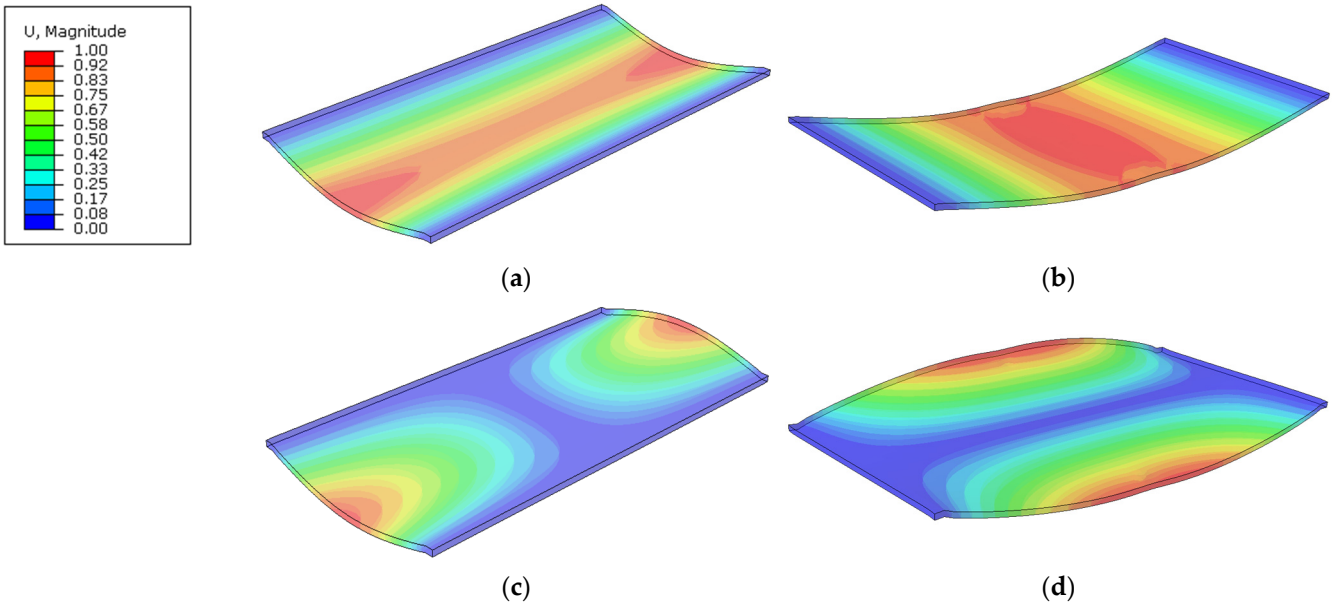

Figure 11. Fundamental shapes for occupied GS1 and GS2 slabs (M = 80 kg), based on linear modal analysis (ABAQUS). (**a**) GS1, mode 1, $f_{1,GS1}$ = 51.2 Hz; (**b**) GS2, mode 1, $f_{1,GS2}$= 14.3 Hz; (**c**) GS1, mode 2, $f_{2,GS1}$ = 53.2 Hz; and (**d**) GS2, mode 2, $f_{2,GS2}$ = 33.2 Hz.

For comparative purposes, a third slab system (CS3) consisting of a reinforced concrete slab with dimensions $A = 5 \times B = 6$ m (150 mm in thickness), with linear supports along B-edges, was also taken into account for further validation [29]. Material properties were taken from [29] and consisted of normal weight concrete with 2350 kg/m^3 density and 38,000 MPa modulus of elasticity. The so-assembled CS3 slab resulted in a total mass of 11,250 kg (R_M = 140 times the volunteer) and in a fundamental beam-like vibration frequency of $f_{1,CS3}$ = 7.23 Hz. A summary of slab features is proposed in Table 5, where λ represents the geometrical slenderness ratio (i.e., effective span over radius of gyration).

Table 5. Features of slabs GS1, GS2, and CS3 for the present investigation (* = occupied structure, with M = 80 kg).

Slab	Material	Size (m^2)	Span (m)	Thickness (m)	Span/Thickness	λ	M_{TOT} (kg)	R_M	f_1 * (Hz)
GS1	Laminated glass	1.35 × 2.65	1.35	0.04352	≈31	107	320	≈4	51.2
GS2	Laminated glass	1.35 × 2.65	2.65	0.04352	≈61	211	320	≈4	14.3
CS3	Concrete	5 × 6	5	0.15	≈33	115	11,250	≈140	7.1

4.2. Loading Strategy and Solving Approach

A set of non-linear dynamic analyses was performed to predict the accelerations in the GS1, GS2, and CS3 slabs, when subjected to random walking excitations. Each numerical analysis consisted of two sub steps, the first one to apply quasistatic permanent loads of structural members, and the second one for the dynamic analysis under pedestrians.

The numerical comparison included, for GS1, GS2, and CS3 systems, two different loading procedures to account for random walks, namely represented by:

- WL1 = a set of FE models in which a single degree of freedom (SDOF) system was rigidly connected to a slab, see Figure 12a, to apply body effects on the base of vertical acceleration time histories (from laboratory experiments in Section 3 and Equation (1)) and a CoM lumped mass representative of the involved volunteer (M = 80 kg). The vertical force transferred by a pedestrian on a substructure can in fact be estimated from Newton's second law of motion, where the dynamic term from experimental input can be expressed as:

$$F(t) = Ma_Z(t) \tag{7}$$

A total of 40 walking configurations were taken into account. The footfall was defined on shell elements to cover a $\approx 0.1 \times 0.1$ m^2 surface.

- WL2 = a set of FE models in which the pedestrian input was described on the base of the deterministic approach in Equation (2), as in Figure 12b, for various walking frequencies f_s. The range 1.5–2.5 Hz was numerically explored (with M = 80 kg and a progressive frequency increase of 0.1 Hz)

A conventional Rayleigh approach was taken into account to define the mass-proportional and stiffness-proportional damping terms [30]. More specifically, they were calculated as:

$$\alpha_0 = \xi \frac{2\omega_1\omega_2}{\omega_1 + \omega_2} \tag{8}$$

$$\beta_0 = \xi \frac{2}{\omega_1 + \omega_2} \tag{9}$$

with ω_1, ω_2 are the natural circular frequencies corresponding to first and second vibration modes (Figure 11). A conventional ξ = 2% damping term was considered for GS1 and GS2.

It should be noted that such a damping value is also in line with average experimental estimates presented in [7,8] for similar LG modular units, belonging to the same case-study system, under single pedestrian walks. For CS3, the reference value ξ = 3% was taken from [29].

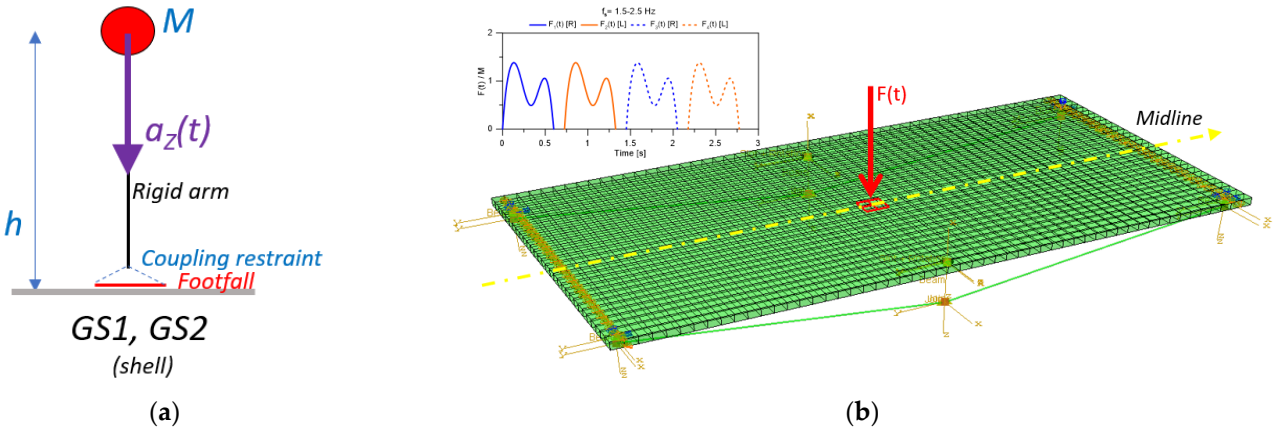

(**a**) (**b**)

Figure 12. Schematic representation of loading strategy for the selected slabs under human-induced effects, as adopted for (**a**) WL1, with SDOF system detail, and (**b**) WL2 procedures (example of GS2 setup).

5. Discussion of Results

The analysis of time domain parametric results was carried out with careful attention to maximum peaks and average trends for critical performance indicators. A total of 150 nonlinear dynamic simulations were carried out in ABAQUS (50 for GS1, 50 for GS2, and 50 for CS3), under WL1 setup (40/each) or WL2 loads (10/each).

Most importantly, the post-processing stage was focused on the comparison of acceleration peaks and trends for the examined systems under the imposed WL1 and WL2 loading protocols. In doing so, based on the two-edge simple support boundaries and the corresponding beam-like bending behavior, the reference control point was set in the center of the slabs.

5.1. GS1 Performance Indicators

The attention was first focused on the GS1 slab system characterized by a relatively high fundamental frequency, and thus less sensitive to possible walk-induced effects. Figure 13a shows the typical distribution of vertical accelerations under the imposed walking paths, while an example of structural acceleration (WL1 input selection) is presented in Figure 13b. As far as the acceleration peaks in a vertical direction ($a_{z,peak}$) or the root-mean-square (RMS) values ($a_{z,RMS}$) taken into account over the time of each simulation, typical results can be seen in Figure 13c,d.

The comparison is carried out by grouping WL1 and WL2 predictions, as a function of the input walking frequency f_s. A linear regression model is also used to assess the general trend of parametric estimates. Most importantly, the effects of walk variability as for WL1 protocol can be noticed in terms of scattered acceleration values, especially for slow motion frequency f_s. Overall, the statistical analysis of parametric results gave evidence of a R-square correlation factor in the order of $R^2 = 0.33$ and $R^2 = 0.64$ for $a_{z,peak}$ and $a_{z,RMS}$, respectively. For GS1 under WL2 deterministic pedestrian loads, such a correlation was estimated in $R^2 = 0.84$ and $R^2 = 0.88$ for $a_{z,peak}$ and $a_{z,RMS}$. Besides the relatively high vibration frequency of GS1 module (Figure 11) and its mostly rigid behavior against human-induced effects, the parametric results give evidence of high variability in body CoM motion parameters and WL1 input, and thus in corresponding effects on a lightweight slab system. At the same time, the WL2 deterministic loads provide single estimates based on pedestrian mass M and waling frequency f_s, but without accounting for additional body and motion features. Globally, it can be noticed in Figure 13c,d that the linear regression models for WL1 and WL2 estimates are mostly coincident, and thus a rather good match of numerical trends on the side of structures can be seen. As far as single walking scenarios are taken into account, on the other side, the WL1 procedure tends to underestimate the structural response as subjected to WL2 pedestrian loads.

5.2. GS2 Performance Indicators

When the GS2 slab configuration under identical WL1 and WL2 loading patterns is taken into account, a bending response as in Figure 14a is obtained, with a substantially different dynamic response compared with GS1. This can also be noticed in Figure 14b, which shows an example of vertical acceleration measured in the center of the slab, under a given body CoM input (WL1), as obtained for GS1 or GS2. A more detailed analysis of numerical results can be observed in Figure 15a,c in the form of a vertical acceleration peak, RMS value, peak-to-peak versus maximum value ratio, and CREST factor (peak to RMS ratio) for the GS2 system.

Differing from Section 5.1, as expected, the lower vibration frequency of the GS2 system (and thus higher sensitivity to walk-induced effects) manifests in largely increased absolute values for the selected performance indicators, especially for walking frequencies $f_s > 1.6$ Hz. In particular, the attention goes on the higher scatter of WL1 and WL2 results for a given frequency f_s. The WL1 loading protocol with linear regression model shows a R-square correlation factor in the order of $R^2 = 0.50$ for $a_{z,peak}$, $R^2 = 0.55$ for $a_{z,RMS}$ in Figure 15a,b, respectively, while WL2 approach gives $R^2 = 0.67$ and $R^2 = 0.65$. Compared with the GS1 system, the GS2 dynamic response is associated to the highest effects when subjected to body CoM input (WL1), rather than the WL2 deterministic loads.

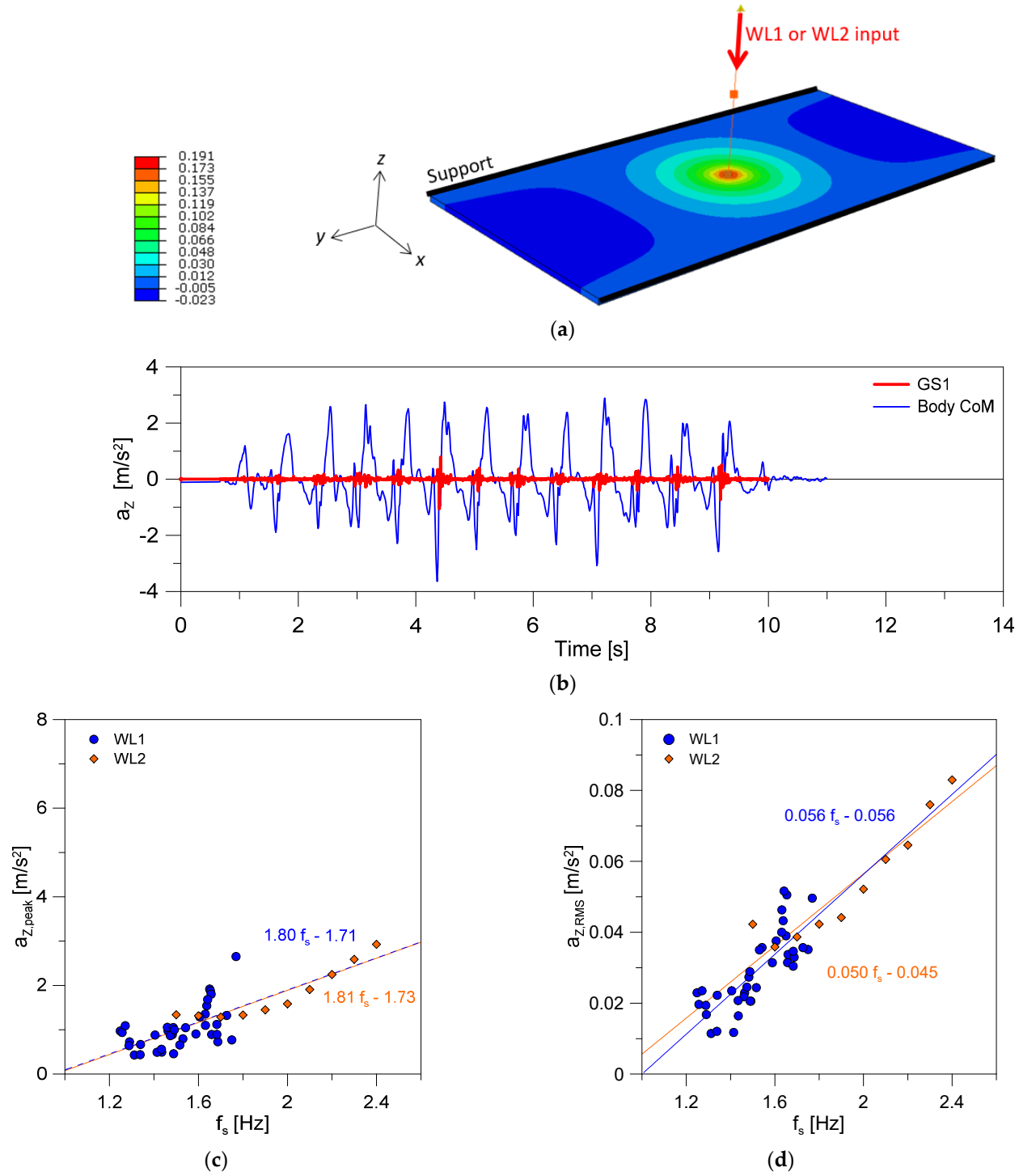

Figure 13. Summary of numerical performance indicators of the GS1 laminated glass slab (ABAQUS): (**a**) typical acceleration distribution (values in m/s^2) with (**b**) example of measured acceleration at the center of the slab (selected record #7 from the total of 40 WL1 input signals), (**c**) peak of vertical acceleration, and (**d**) RMS value.

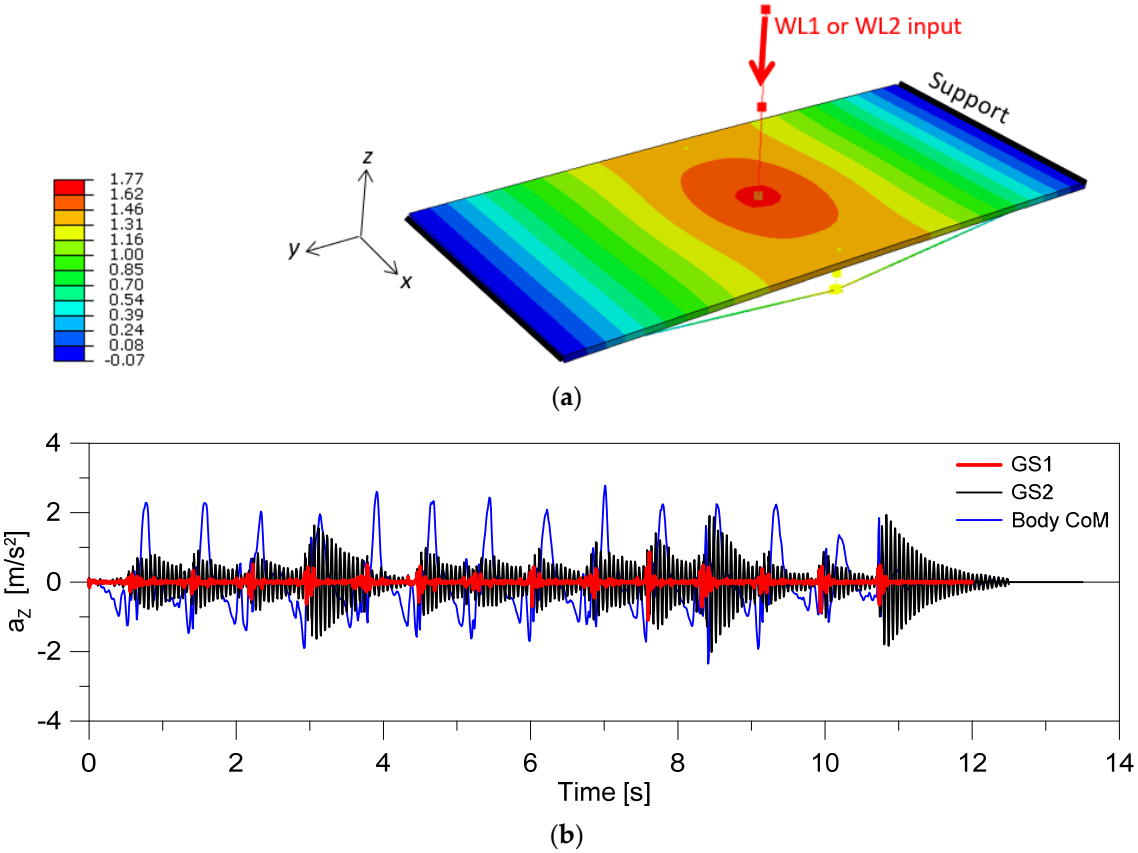

Figure 14. Dynamic response of the GS2 laminated glass slab (ABAQUS): (**a**) typical acceleration distribution (values in m/s^2), with (**b**) example of measured acceleration at the center of the slab (selected record #14 from the total of 40 WL1 input signals).

In Figure 15a, "Field Test" data from [9] are also reported for further assessment of present numerical outcomes. Yellow dots are in fact representative of three vertical acceleration peaks measured for the real GS2 structure (in-service walkway) under in-place jumps (center of slab) from the herein involved volunteer. As shown, for low walking frequency (f_s = 1.24 Hz), both WL1 and WL2 are in the same order of magnitude of few experimental measures, but the WL2 procedure tends to underestimate the maximum structural effects of random walks ($\approx -7.8\%$ the scatter of WL1 loading scheme towards the mean experimental value, and $\approx -16\%$ for the WL2 configuration, on the unconservative side). Besides, even under intrinsic limitations due to the number of field experimental samples, neither the WL1 approach nor the WL2 loading scheme are able to capture the overall linear trend of "Field Test" acceleration peaks. For higher frequency (f_s = 1.8 Hz), both the WL1 and WL2 numerical outcomes underestimate the field measurement on the GS2 structure. A slightly improved match of field experimental trends is offered by the GS2 assembly subjected to uncoupled WL1 input, with $\approx -20\%$ of the scatter to the experimental value, while the WL2 output is even more conservative ($\approx -40\%$). The magnitude of the CREST factor in Figure 15d, finally, is also representative of a rather impulsive response of the GS2 system under input walks, but highly scattered with f_s due to slab sensitivity to motion variability.

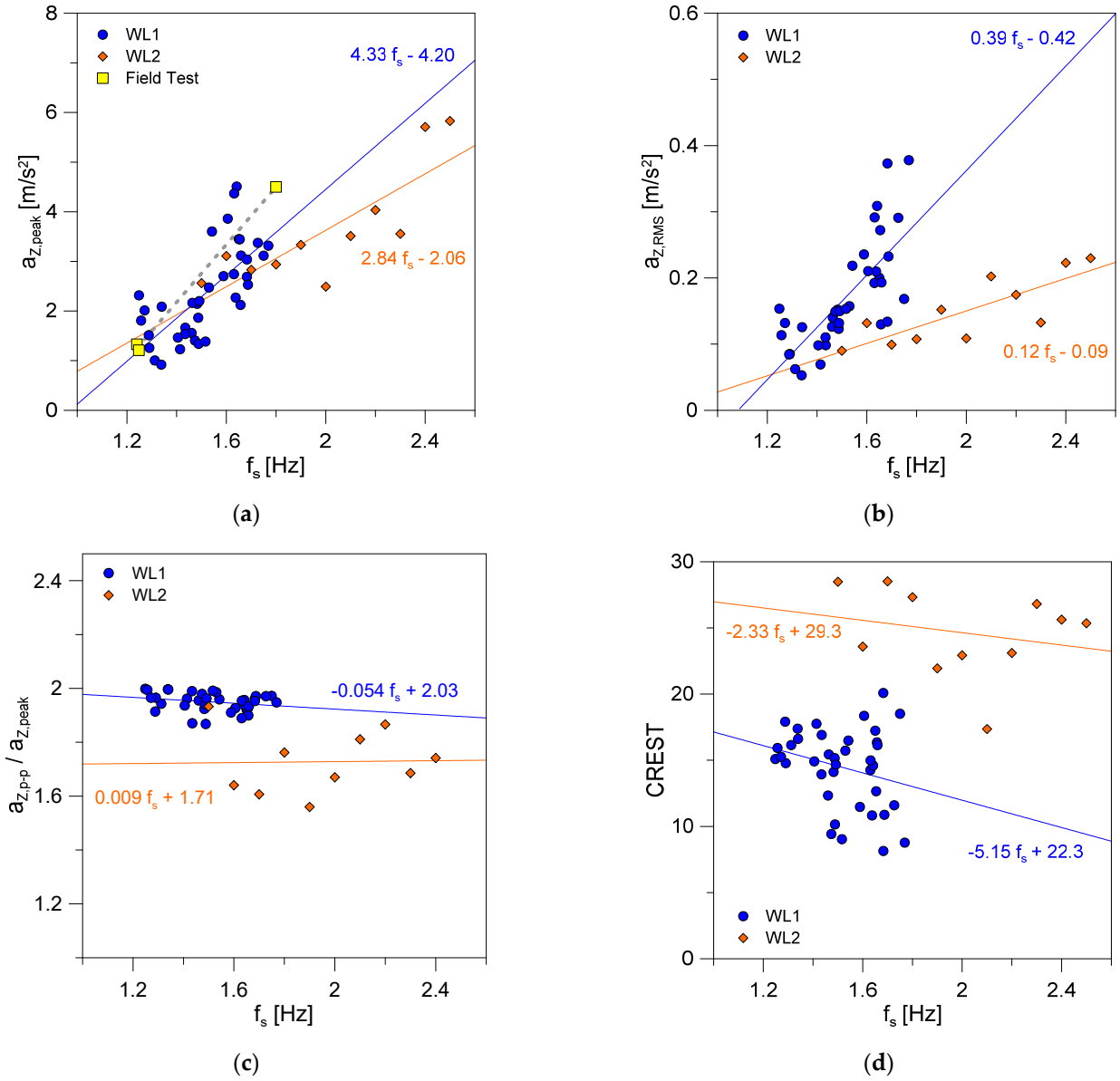

Figure 15. Summary of numerical performance indicators of the GS2 laminated glass slab (ABAQUS): (**a**) peak of vertical acceleration, (**b**) RMS value, (**c**) peak-to-peak versus maximum value ratio, and (**d**) CREST factor.

5.3. CS3 Performance Indicators

The concrete CS3 slab inspired by [29] was also investigated. To this aim, the present FE numerical approach was first validated towards data discussed in [29], both in terms of linear modal analysis and nonlinear dynamic simulations under WL2 pedestrian loads (and a superimposed accidental load Q = 4.84 kN/m^2 for offices [29]), see Figure 16.

In this regard, Figure 16a shows the fundamental vibration frequency for the first six vibration modes of the CS3 system, as obtained from the present numerical investigation or in [29]. Further comparisons are proposed for concrete slabs similar to CS3, but characterized by total thickness in the order of 0.1 m or 0.2 m, respectively. Figure 16b,c, moreover, show the fundamental vibration shapes of the system. Additional validation of the herein proposed loading and solving strategy (Section 4.2) can be noticed in Figure 16d, where $a_{Z,RMS}$ values for the CS3 system under WL2 pedestrian loads are presented.

The numerical results for CS3 system under WL1 or WL2 pedestrian input are summarized in Figure 17, with evidence of typical acceleration distribution in Figure 17a, at a

selected time instant, and other relevant performance indicators in Figure 17b–d in terms of absolute acceleration peak, RMS value, and peak-to-peak versus maximum value ratio.

The WL1 loading protocol with linear regression model shows a *R*-square correlation factor in the order of $R^2 = 0.49$ for $a_{z,peak}$ and $R^2 = 0.50$ for $a_{z,RMS}$ ($R^2 = 0.09$ for $a_{z,p\text{-}p}/a_{z,peak}$), while the WL2 approach gives $R^2 = 0.72$, $R^2 = 0.69$, and $R^2 = 0.04$. As observed for previous selected slabs, the dynamic response of the CS3 system was found associated to the highest vibration effects when subjected to body CoM input (WL1), rather than WL2 deterministic loads reproducing the effects of the involved volunteer. Furthermore, it is worth noting that for a given walking frequency fs, the scattered distribution of calculated performance indicators is based on the WL1 procedure, as compared with a single response value based on the WL2 calculation approach.

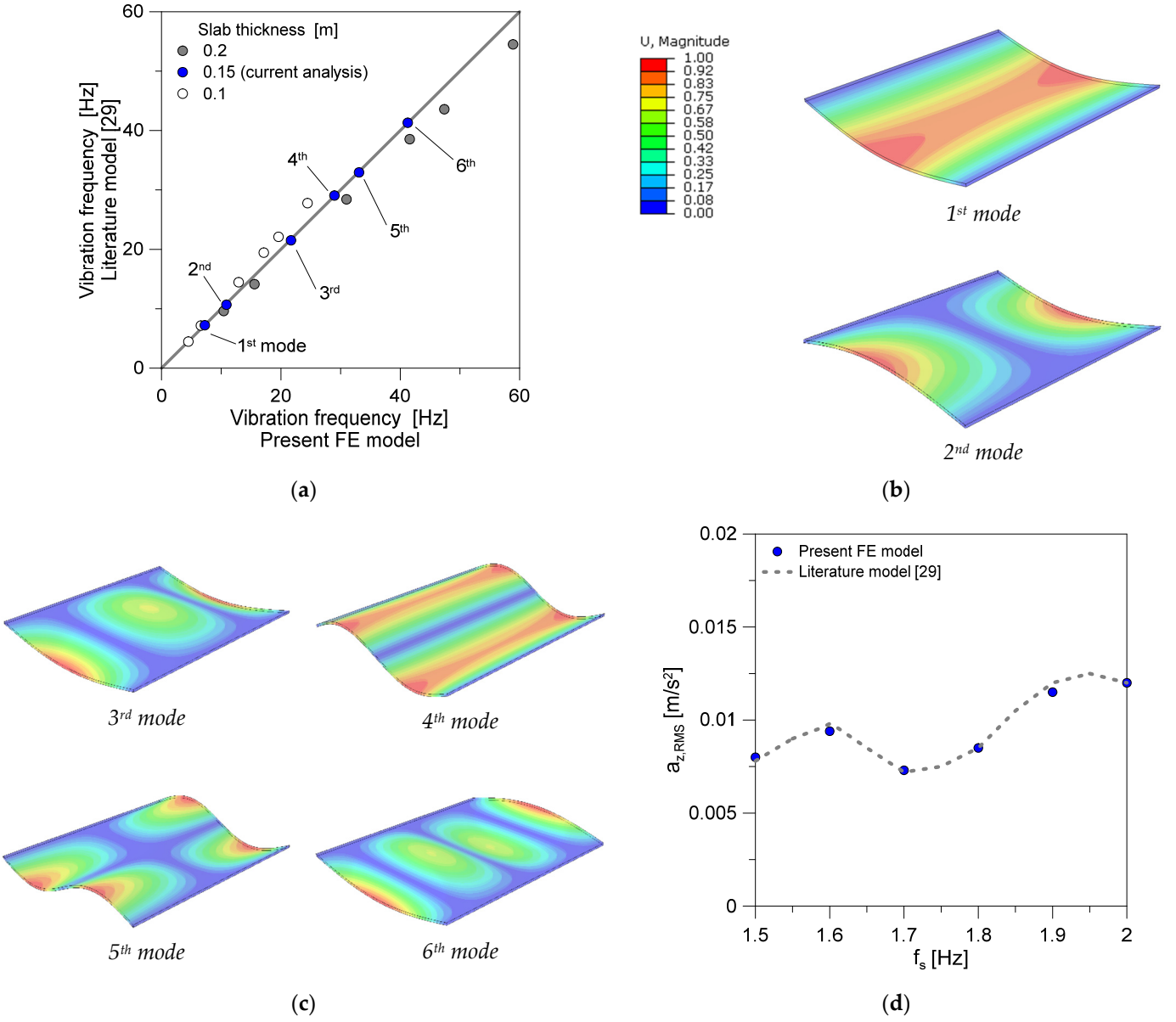

Figure 16. Validation of the present FE model strategy for the CS3 slab (ABAQUS): (**a**) fundamental vibration frequencies, (**b**,**c**) corresponding modal shapes, and (**d**) $a_{Z,RMS}$ trends for CS3 under WL2 pedestrian loads.

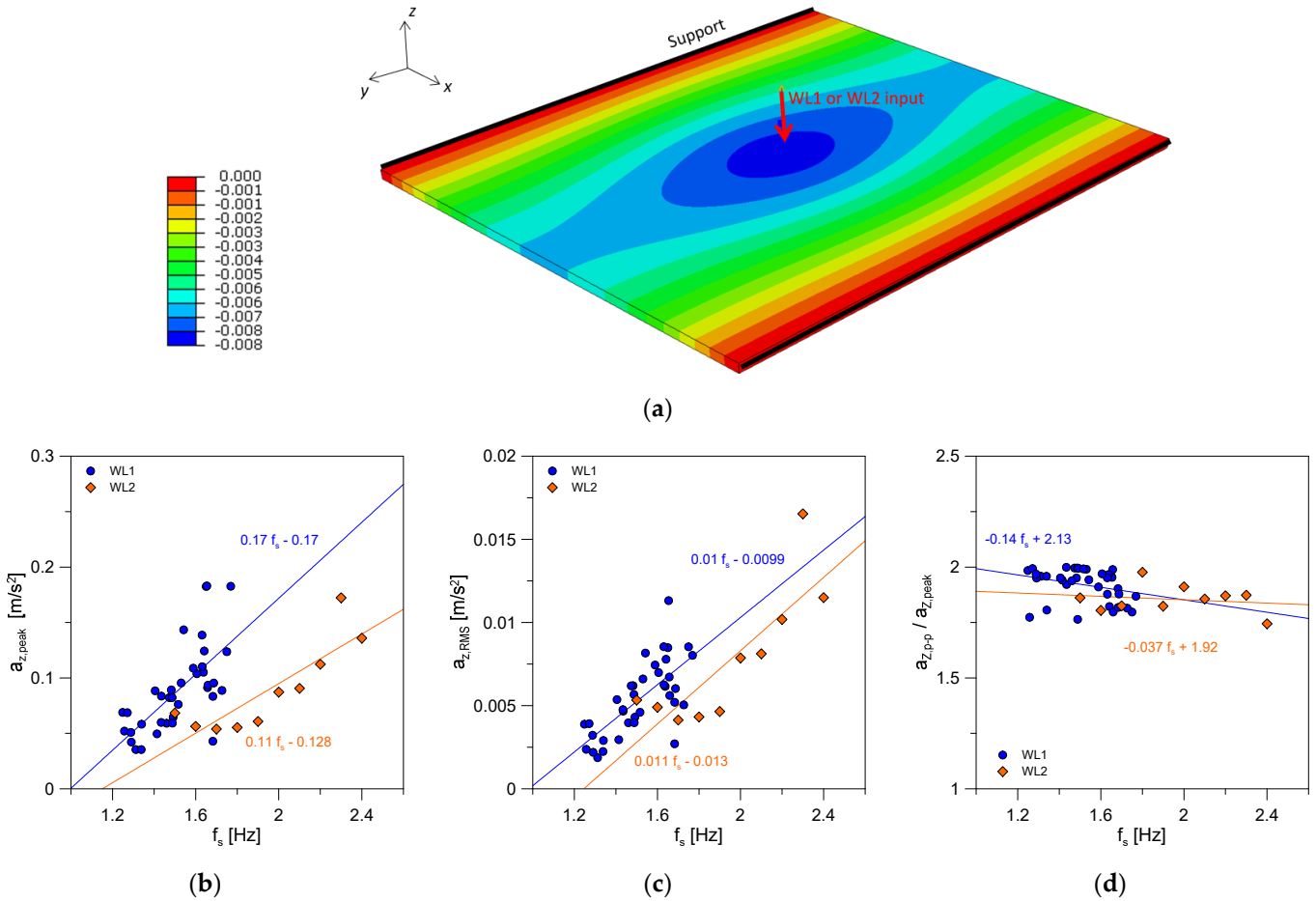

Figure 17. Summary of numerical performance indicators of the CS3 concrete slab (ABAQUS): (**a**) typical acceleration distribution (values in m/s^2), with (**b**) peak of vertical acceleration, (**c**) RMS value, and (**d**) peak-to-peak versus maximum value ratio.

6. Conclusions

The vibration analysis of the pedestrian system, especially for lightweight and/or slender slabs which are highly sensitive to walk-induced effects, represents an open challenge for designers. In this paper, the attention was focused on typically slender laminated glass (LG) slabs that are used in buildings to cover wide transparent pedestrian surfaces, under variable boundaries and modular dimensions. As is known, consolidated deterministic models are available in the literature to efficiently describe and verify the load effects due to pedestrians walking on structures. Besides, these models are rather approximate because they account for the mass of pedestrians and walking frequency only.

In this regard, an original experimental and numerical investigation was proposed to address the potential of uncoupled body measures for a realistic vibration analysis of slender slabs. More specifically, 40 original laboratory experimental records were presented for vibration serviceability purposes, as obtained in terms of body center of mass (CoM) acceleration time histories for a walking volunteer moving on a rigid substrate, when equipped by a single Wi-Fi sensor based on micro electromechanical systems (MEMS) technology. The collected laboratory CoM records, once post-processed and expressed in terms of vertical acceleration components in time, were used as key input for finite element (FE) nonlinear vibration analysis in time domain (WL1) of three different slab configurations, two of them made of laminated glass (GS1 and GS2) and characterized by identical geometrical and mechanical properties, but different boundaries (and thus fundamental frequency and sensitivity to walks), and a third reinforced concrete slab from literature (CS3). The numerical analysis of GS1, GS2, and CS3 systems included a total

of 150 nonlinear dynamic simulations. Their dynamic response was assessed towards numerical parametric results based on literature deterministic approaches to account for walk-induced effects (WL2), as well as to past field experiments (GS2 only) for the same volunteer walking on the real GS2 system.

As shown, the structural frequency is relatively high (as for GS1, with $f_{1,GS1}$ = 51.2 Hz) and both WL1 and WL2 procedures result in rather equal average performance indicators on the structural side (vertical acceleration peak, RMS value, etc.). On the other side, for the GS2 system characterized by lower but still not critical vibration frequency ($f_{1,GS2}$ = 14.3 Hz), more pronounced scattered trends were collected on the structure, with both WL1 and WL2 parametric simulations. Most importantly, the WL1 outcomes were observed to have a better correlation with few field experimental data, which were used to support the comparative discussion of numerical results. Conversely, the collected WL2 estimates were placed on the unsafe side. Finally, the concrete slab (CS3) characterized by low vibration frequency ($f_{1,CS3}$ = 7.1 Hz) but significantly high structural mass, gave evidence of more pronounced vibration effects based on WL1 loading protocol, rather than WL2 procedure.

In this sense, the present study proved that simple Wi-Fi body CoM measurements based on a single sensor can offer useful feedback and input for the structural analysis and vibration serviceability assessment of slender slab systems, as highlighted for the selected configurations. Especially for LG slabs, which are typically characterized by high slenderness and relatively small structural mass, compared with occupants, the use of simplified loading protocols may result in unconservative structural estimates. Furthermore, the study proved that the LG slab system, even when characterized by a relatively high structural vibration frequency (such as GS1), may suffer from high sensitivity to walk-induced effects, compared with other constructional solutions, and thus require even more attention for monitoring purposes.

Author Contributions: C.B.: conceptualization, methodology, software, validation, formal analysis, investigation, resources, data curation, writing—original draft preparation, and project administration. S.N.: methodology and validation. All authors have read and agreed to the published version of the manuscript.

Funding: This research received no external funding.

Institutional Review Board Statement: Not applicable.

Informed Consent Statement: Not applicable.

Data Availability Statement: Supporting data will be shared upon request.

Conflicts of Interest: The author declares no conflict of interest.

References

1. *CEN/TC 250*; prCEN/TS xxxx-1: 2019—In-Plane Loaded Glass Components. CEN—European Committee for Standardization: Brussels, Belgium, 2019.
2. *CEN/TC 250*; prCEN/TS xxxx-2: 2019—Out of-Plane Loaded Glass Components. CEN—European Committee for Standardization: Brussels, Belgium, 2019.
3. *CNR-DT 210/2013*; Istruzioni Per la Progettazione, L'esecuzione ed il Controllo di Costruzioni con Elementi Strutturali di Vetro. National Research Council of Italy (CNR): Roma, Italy, 2013. (In Italian)
4. Zemanová, A.; Zeman, J.; Janda, T.; Schmidt, J.; Šejnoha, M. On modal analysis of laminated glass: Usability of simplified methods and Enhanced Effective Thickness. *Compos. Part B Eng.* **2018**, *151*, 92–105. [CrossRef]
5. Zemanová, A.; Zeman, J.; Šejnoha, M. Comparison of viscoelastic finite element models for laminated glass beams. *Int. J. Mech. Sci.* **2017**, *131-132*, 380–395. [CrossRef]
6. Bedon, C. Issues on the Vibration Analysis of In-Service Laminated Glass Structures: Analytical, Experimental and Numerical Investigations on Delaminated Beams. *Appl. Sci.* **2019**, *9*, 3928. [CrossRef]
7. Bedon, C. Experimental investigation on vibration sensitivity of an indoor glass footbridge to walking conditions. *J. Build. Eng.* **2020**, *29*, 101195. [CrossRef]
8. Bedon, C. Diagnostic analysis and dynamic identification of a glass suspension footbridge via on-site vibration experiments and FE numerical modelling. *Compos. Struct.* **2019**, *216*, 366–378. [CrossRef]

9. Bedon, C.; Noè, S. Post-Breakage Vibration Frequency Analysis of In-Service Pedestrian Laminated Glass Modular Units. *Vibration* **2021**, *4*, 836–852. [CrossRef]
10. Gong, M.; Li, Y.; Shen, R.; Wei, X. Glass Suspension Footbridge: Human-Induced Vibration, Serviceability Evaluation, and Vibration Mitigation. *J. Bridg. Eng.* **2021**, *26*, 05021014. [CrossRef]
11. Sedlacek, G.; Heinemeyer, C.; Butz, C. *Generalisation of Criteria for Floor Vibrations for Industrial, Office, Residential and Public Building and Gymnasium Halls*; European Commission: Luxembourg, 2006.
12. Bachmann, H.; Ammann, W. Vibrations in structures induced by man and machines. *Can. J. Civ. Eng.* **1987**, *15*, 1086–1087.
13. Shahabpoor, E.; Pavic, A.; Racic, V. Interaction between Walking Humans and Structures in Vertical Direction: A Literature Review. *Shock Vib.* **2016**, *2016*, 3430285. [CrossRef]
14. Miyazaki, S. Long-term unrestrained measurement of stride length and walking velocity utilizing a piezoelectric gyroscope. *IEEE Trans. Biomed. Eng.* **1997**, *44*, 753–759. [CrossRef]
15. Veltink, P.H.; Bussmann, H.B.J.; De Vries, W.; Martens, W.L.J.; Van Lummel, R.C. Detection of static and dynamic activities using uniaxial accelerometers. *IEEE Trans. Rehabil. Eng.* **1996**, *4*, 375–385. [CrossRef]
16. Sabatini, A.M.; Martelloni, C.; Scapellato, S.; Cavallo, F. Assessment of Walking Features from Foot Inertial Sensing. *IEEE Trans. Biomed. Eng.* **2005**, *52*, 486–494. [CrossRef]
17. Van Nimmen, K.; Lombaert, G.; Jonkers, I.; De Roeck, G.; Van den Broeck, P. Characterisation of walking loads by 3D inertial motion tracking. *J. Sound Vib.* **2014**, *333*, 5212–5226. [CrossRef]
18. Van Nimmen, K.; Zhao, G.; Seyfarth, A.; Van den Broeck, P. A Robust Methodology for the Reconstruction of the Vertical Pedestrian-Induced Load from the Registered Body Motion. *Vibration* **2018**, *1*, 250–268. [CrossRef]
19. Bocian, M.; Brownjohn, J.; Racic, V.; Hester, D.; Quattrone, A.; Monnickendam, R. A framework for experimental determination of localised vertical pedestrian forces on full-scale structures using wireless attitude and heading reference systems. *J. Sound Vib.* **2016**, *376*, 217–243. [CrossRef]
20. Simonetti, E.; Bergamini, E.; Vannozzi, G.; Bascou, J.; Pillet, H. Estimation of 3D Body Center of Mass Acceleration and Instantaneous Velocity from a Wearable Inertial Sensor Network in Transfemoral Amputee Gait: A Case Study. *Sensors* **2021**, *21*, 3129. [CrossRef]
21. Busca, G.; Cappellini, A.; Manzoni, S.; Tarabini, M.; Vanali, M. Quantification of changes in modal parameters due to the presence of passive people on a slender structure. *J. Sound Vib.* **2014**, *333*, 5641–5652. [CrossRef]
22. Setareh, M.; Gan, S. Vibration testing, analysis and human-structure interaction studies of a slender footbridge. *J. Perform. Constr. Facil.* **2018**, *32*, 040018068. [CrossRef]
23. Muhammad, Z.; Reynolds, P.; Avci, O.; Hussein, M. Review of Pedestrian Load Models for Vibration Serviceability Assessment of Floor Structures. *Vibration* **2019**, *2*, 1–24. [CrossRef]
24. Bedon, C.; Fasan, M. Reliability of field experiments, analytical methods and pedestrian's perception scales for the vibration serviceability assessment of an in-service glass walkway. *Appl. Sci.* **2019**, *9*, 1936. [CrossRef]
25. Bedon, C.; Mattei, S. Facial Expression-Based Experimental Analysis of Human Reactions and Psychological Comfort on Glass Structures in Buildings. *Buildings* **2021**, *11*, 204. [CrossRef]
26. *BeanDevice® Wilow® User Manual—Wilow® Wireless Sensor*, version 2.3.2; BenAir: Berlin, Germany, 2019.
27. Bedon, C.; Bergamo, E.; Izzi, M.; Noé, S. Prototyping and Validation of MEMS Accelerometers for Structural Health Monitoring—The Case Study of the Pietratagliata Cable-Stayed Bridge. *J. Sens. Actuator Netw.* **2018**, *7*, 30. [CrossRef]
28. *ABAQUS Computer Software v.6.14*; Simulia: Dassault, RI, USA, 2021.
29. Cai, Y.; Gong, G.; Xia, J.; He, J.; Hao, J. Simulations of human-induced floor vibrations considering walking overlap. *SN Appl. Sci.* **2019**, *2*, 19. [CrossRef]
30. Clough, R.W.; Penzien, J. *Dynamics of Structures*; McGrawHill: Berkeley, CA, USA, 1993.